Statistical Characterization of GPS Signal-In-Space Errors

Liang Heng, Grace Xingxin Gao, Todd Walter, and Per Enge,
Stanford University

BIOGRAPHY

Liang Heng is a Ph.D. candidate under the guidance of Professor Per Enge in the Department of Electrical Engineering at Stanford University. He received his B.S. and M.S. degrees in electrical engineering from Tsinghua University, Beijing, China. His current research interests include GNSS integrity and modernization.

Grace Xingxin Gao, Ph.D., is a research associate in the GPS lab of Stanford University. She received the B.S. degree in mechanical engineering and the M.S. degree in electrical engineering, both at Tsinghua University, Beijing, China. She obtained the Ph.D. degree in electrical engineering at Stanford University. Her current research interests include GNSS signal and code structures, GNSS receiver architectures, and interference mitigation. She has received the Institute of Navigation (ION) Early Achievement Award.

Todd Walter, Ph.D., is a senior research engineer in the Department of Aeronautics and Astronautics at Stanford University. He received his Ph.D. from Stanford and is currently working on the Wide Area Augmentation System (WAAS), defining future architectures to provide aircraft guidance, and working with the FAA and GPS Wing on assuring integrity on GPS III. Key early contributions include prototype development proving the feasibility of WAAS, significant contribution to WAAS MOPS, and design of ionospheric algorithms for WAAS. He is a fellow of the Institute of Navigation.

Per Enge, Ph.D., is a Professor of Aeronautics and Astronautics at Stanford University, where he is the Kleiner-Perkins, Mayfield, Sequoia Capital Professor in the School of Engineering. He directs the GPS Research Laboratory, which develops satellite navigation systems based on the Global Positioning System (GPS). He has been involved in the development of WAAS and LAAS for the FAA. Per has received the Kepler, Thurlow and Burka Awards from the ION for his work. He is also a Fellow of the ION and the Institute of Electrical and Electronics Engineers (IEEE). He received his PhD from the University of Illinois in 1983.

ABSTRACT

For most Global Positioning System (GPS) standard positioning service (SPS) users, real-time satellite orbits and clocks are derived from predicted ephemeris and clock parameters in broadcast navigation messages. Broadcast ephemeris and clock errors, the differences between the broadcast orbits/clocks and the truth, account for a dominant portion of signal-in-space (SIS) errors. Traditionally, SIS user range errors (UREs) is assumed to follow a zero-mean normal distribution with standard deviation represented by the broadcast user range accuracy (URA). In addition, advanced receiver autonomous integrity monitoring (ARAIM) may rely on an assumption that UREs of different satellites are uncorrelated. This paper is intended to examine these assumptions and give a thorough characterization of core SIS error behavior based on the statistics of recent data.

The radial, alongtrack, and crosstrack ephemeris errors and clock errors are computed by comparing the broadcast ephemerides/clocks with the precise ones, followed by the generation of instantaneous SIS UREs, global-average SIS UREs, and worst-case SIS UREs. Anomalous satellite behaviors are identified and excluded by an outlier filter. Robust statistics techniques are implemented to avoid the impact of statistical outliers.

An analysis of long-term stationarity is first carried out to determine the range of useful data. The SIS errors are then characterized with respect to mean and standard deviation, spatial correlation, normality, relation between rms URE and URA, and correlation among different satellites. The results show that mean of SIS errors are nonzero for several satellites; the radial errors, alongtrack errors, and clock errors are relatively strongly correlated; UREs usually have a non-Gaussian distribution; different satellites have different interpretation of URA; and the UREs of different satellites are slightly correlated.

INTRODUCTION

The Global Positioning System (GPS) is so far the most widely used space-based global positioning, navigation, and timing system. GPS works on the principle of trilateration, in which the measured distance from a user receiver to at least four GPS satellites in view as well as the positions and clocks of these satellites are the prerequisites for the user receiver to fix its exact position [1]. For most GPS standard positioning service (SPS) users, real-time satellite positions and clocks are derived from ephemeris parameters and clock correction terms in navigation messages broadcast by GPS satellites. The GPS Control Segment routinely generates navigation message data on the basis of a prediction model and the measurements at more than a dozen monitor stations [2]. The differences between the broadcast ephemerides/clocks and the truth account for signal-in-space (SIS) errors. SIS errors are mainly contributed by the errors due to the

- Space Segment, such as satellite acceleration uncertainty, clock instability, satellite antenna variation [3], and signal imperfection [4], and the errors due to the
- Control Segment, such as the estimation errors, prediction errors, and curve fit errors in broadcast ephemerides and clocks [5].

Therefore, SIS errors are difficult to describe because they are neither purely stochastic nor purely deterministic.

However, characterization and estimation of the core SIS error behavior are of vital importance for GPS SIS integrity. For example, receiver autonomous integrity monitoring (RAIM) (or Advanced RAIM (ARAIM) [6]) and GPS III integrity may rely on the following assumptions:

- Mean of SIS errors is close to zero;
- User range errors (UREs) are described or overbounded by a normal distribution;
- Expected root mean square (rms) UREs are represented by broadcast user range accuracy (URA);
- UREs of different satellites are uncorrelated.

There have been some prior work studying GPS SIS errors [7–11], but the most of them did not focus on examining the above assumptions. Employing the similar philosophy and methodology as our previous paper that studies anomalous SIS error behavior [12, 13], this paper will examine the above assumptions and give a thorough characterization of core SIS error behavior based on the statistics of recent data. For the rest of this paper, we start with a description of the methodology and then elaborate on the statistical characterizations.

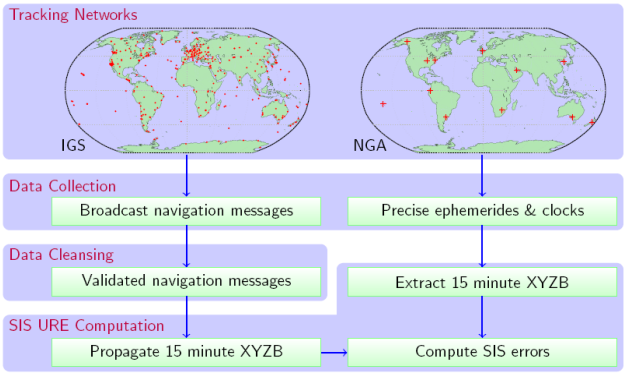

Figure 1. Procedure for computing SIS errors.

METHODOLOGY

Computation of ephemeris and clock errors

GPS ephemeris/clock errors are computed by comparing the broadcast ephemerides/clocks with the precise, post-processed ones. As shown in Figure 1, broadcast navigation message data are obtained from International GNSS Service (IGS) [14]. Our well-established data cleansing software is employed to generate validated navigation messages that are free of data logging errors [12, 13]. Precise ephemerides/clocks from National Geospatial-Intelligence Agency (NGA) are available every 15 minutes synchronized to GPS time [15]. NGA precise ephemerides/clocks are regarded as truth because they are an order of magnitude or more accurate than the broadcast ephemerides/clocks [16].

The validated navigation messages are used to propagate broadcast orbits/clocks at 15-minute intervals that coincide with the precise ephemerides/clocks. The differences between broadcast and precise ephemerides are the ephemeris errors, which are represented in the reference frame with respect to the space vehicle: R—radial, A—alongtrack, and C—crosstrack. The differences between broadcast and precise clocks are the clock errors, denoted by T in meters.

SIS URE metrics

GPS SIS URE is the pseudorange inaccuracy due to ephemeris and clock errors. For an arbitrary set of ephemeris and clock errors (R, A, C, T), GPS receivers at different locations on the Earth may experience different SIS UREs. Accordingly, the following four SIS URE metrics are considered in this paper:

- Instantaneous SIS UREs computed for 20 points spread evenly on the earth (Figure 2);
- Global average rms SIS URE given by [5]

$$\sqrt{(0.98R - T)^2 + 0.141^2(A^2 + C^2)}; \qquad (1)$$

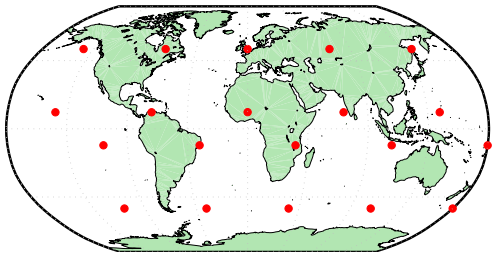

Figure 2. Instantaneous UREs are computed for 20 points spread evenly on the earth, which are derived from the vertices of a regular dodecahedron.

- Orbit-error-only rms SIS URE_O defined as
$$\sqrt{(0.98R)^2 + 0.141^2(A^2 + C^2)}; \tag{2}$$
- Worst-case SIS URE defined as
$$\max_{|\theta|\le 13.88^\circ} (R\cos\theta - T + \sqrt{A^2 + C^2}\sin\theta), \tag{3}$$
where $\max(x)$ maximizes $|x|$ and return the corresponding x.

Worst-case URE can be computed either numerically from instantaneous UREs or analytically from (R, A, C, T) [12]. In this paper we use the latter way.

Outlier filter

Not all the SIS errors computed above should be included in the statistics. For example, GPS receivers usually do not use broadcast ephemerides/clocks that are set unhealthy or older than 4 hours. The *GPS SPS Performance Standard* [5] has defined a SIS not-to-exceed URE (NTE) tolerance: 4.42 times URA upper bound (UB)[1] Accordingly, the SIS errors that meet any one of the following conditions are not included in our analysis:

- The corresponding broadcast navigation message is unhealthy, i.e.,
  - Health status word is not zero, or
  - URA is greater than 48 meters [5];
- The corresponding broadcast navigation message is not in its 4-hour fit interval;
- The corresponding precise ephemeris/clock is missing or marked "event";
- The corresponding worst-case URE exceeds the NTE tolerance.

For a thorough discussion of these criteria and the anomalous SIS behavior in the past, please refer to [12, 13].

[1] For a normal distribution, ±4.42-sigma is equivalent to 10^{-5} tail probability. Although the UREs generally have a heavier tail than a normal distribution, the NTE tolerance is still a conservative threshold for outlier filter because URA UB is at least two times larger than the standard deviation of UREs.

Robust statistics

Because SIS errors do not necessarily have a normal distribution, the traditional statistics such as sample mean and sample standard deviation may be affected by some extreme samples or remaining outliers[2]. To cope with this problem, we use trimmed mean (also referred to as truncated mean) to measure the central tendency. A trimmed mean function $\text{mean}_\alpha(\cdot)$ is the mean after discarding the samples at the $50\alpha\%$ high end and $50\alpha\%$ low end. Analogously, a trimmed standard deviation function is defined as
$$\text{std}_\alpha(X) = \sqrt{\text{mean}_\alpha((X - \text{mean}_\alpha(X))^2)}. \tag{4}$$
In fact, trimmed mean is a compromise between sample mean and sample median, and trimmed standard deviation a compromise between sample standard deviation and sample median absolute deviation. In this paper, we use a small value $\alpha = 0.01$, i.e., use 99% of the data, to make the result close to the mean or the standard deviation.

Normality metric

SIS errors are usually described or overbounded by a normal distribution. Hence, it is important to know how close the real errors are to normally distributed. Popular statistical hypothesis tests of normality, such as Shapiro-Wilk test [17], Lilliefors test [18], and Jarque-Bera test [19], are so strict that they usually reject the null hypothesis that the SIS error samples comes from a distribution in the normal family. Even worse, these tests can not return a meaningful p-value to tell how far the samples are from normally distributed. Therefore, kurtosis is proposed to to quantify normality. Kurtosis (or excess kurtosis) is defined as
$$\gamma(X) = \frac{\mathbb{E}(X - \mathbb{E}X)^4}{(\mathbb{E}(X - \mathbb{E}X)^2)^2} - 3. \tag{5}$$
A normal distribution has kurtosis $\gamma = 0$; a sub Gaussian distribution with a lighter tail usually has kurtosis $\gamma < 0$; a super Gaussian distribution with a heavier tail usually has kurtosis $\gamma > 0$.

Since kurtosis involves 4th-order statistics, it relies on extreme values but is vulnerable to statistical outliers. Therefore, we use a two-step outlier filter. In the first step, the samples with the absolute value greater than 30 meters are discarded. 30 meters is greater than 15-sigma for most SIS errors, so any samples beyond this threshold must be statistical outliers. In the second step, 0.01% upper and lower ends are trimmed, i.e., 99.99% samples are involved in kurtosis computation, which is important for a correct kurtosis estimation [20].

[2] Moreover, the sample mean may not be a maximum likelihood (ML) estimator of expected value for non-Gaussian samples. For instance, sample median, rather than sample mean, is the ML estimator of expected value for the samples from a two-sided exponential distribution.

STATISTICAL CHARACTERIZATION

Long-term stationarity

For the methodology and objective of this paper, any meaningful statistics should be based on a range of data that are relatively stationary. Figure 3 shows the daily median of global average rms SIS URE, orbit-error-only URE_O, and absolute value of clock errors for two GPS satellites. The long-term performance of IIR Space Vehicle Number (SVN) 47 is very typical, and a similar improving trend of SIS performance can be seen for all other GPS satellites except IIA SVN 27, which has a rather unusual worsening trend.

Two key messages are revealed from Figure 3. One is that the SIS performance is dominated by the clock performance, and the clock performance may affect the ephemeris performance. The other is that the long-term performance, for both typical and atypical, was not stationary during the last 7 years. Therefore, the statistics in the rest of the paper will base on the data of last 3 years because the performance

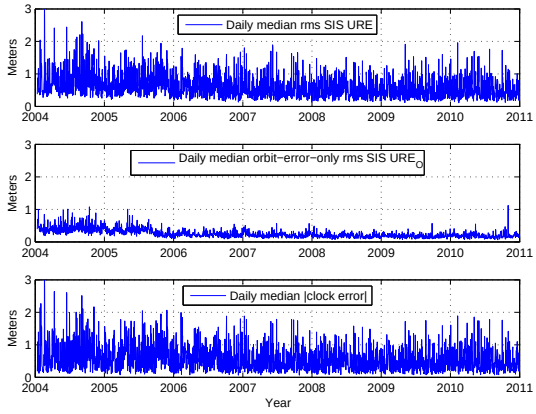

(a) Typical long-term performance: IIR SVN 47/PRN22

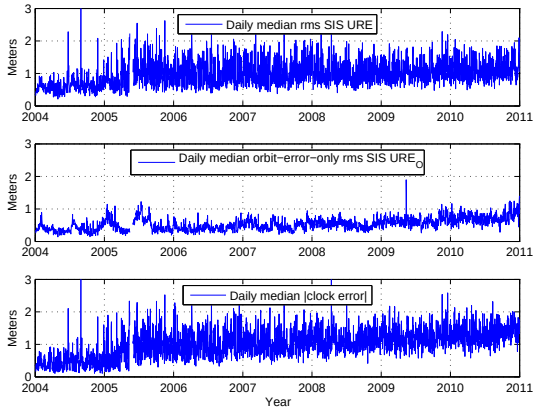

(b) Atypical long-term performance: IIA SVN 27/PRN 27

Figure 3. Daily rms of global average rms SIS URE, orbit-error-only URE_O, and absolute value of clock errors.

was relatively stationary and $3\times365\times24\times4 \approx 10^5$ samples per satellite are adequate for the statistical confidence of the core SIS error behavior.

Mean and standard deviation of SIS errors

Although ephemeris errors are generally assumed to have a zero mean distribution, the reality may be different. Figure 4 plots the means of ephemeris errors, clock errors, instantaneous UREs, and worse-case UREs with a comparison to their standard deviations. The satellites are arranged roughly chronologically according to their Block Type[3] and SVN along the y-axis.

Figure 4 tells many stories. First of all, almost all satellites have zero mean for their crosstrack errors, while about one third satellites have significant nonzero mean for their along-

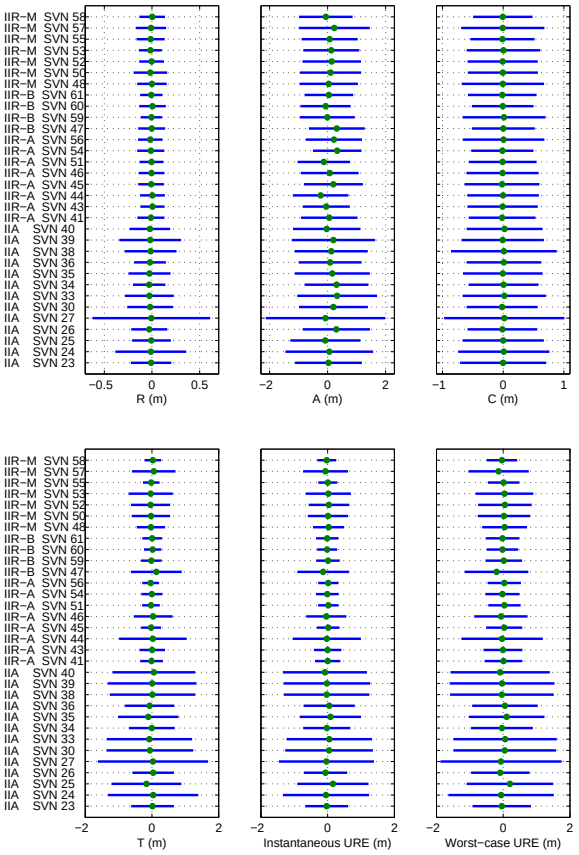

Figure 4. Mean of various SIS errors with a comparison to standard deviation. The blue line with a length of twice the standard deviation is centered at the mean denoted by the green dot.

[3]In the figure, we follow the IGS convention to subdivide IIR satellites into two subgroups IIR-A and IIR-B because the last four IIR satellites were equipped with improved antennas. [21]

track errors. Fortunately, nonzero alongtrack or crosstrack errors do not result in nonzero mean of UREs. The mean of UREs are mainly correlated with the mean of clock errors and radial errors. The nonzero mean of UREs is not critical to ARIAM because no satellite has a mean exceeding 0.2 times standard deviation.

Secondly, in light of standard deviation, the IIR and IIR-M satellites usually have a better SIS performance than IIA. Table 1 summaries the standard deviation of various SIS errors grouped by Block Type. The better SIS performance of the young satellites is mainly due to better onboard clocks and better radial estimation. Nevertheless, SIS error behavior is different from satellite to satellite even for those within the same block and of similar age. A precise model for SIS errors should treat each satellite individually.

Lastly, both Figure 4 and Table 1 imply that clock performance dominates the performance of SIS UREs, reinforcing our observation from the long-term behavior.

	IIA	IIR	IIR-M
Radial (m)	0.243	0.130	0.145
Alongtrack (m)	1.258	0.921	1.000
Crosstrack (m)	0.675	0.575	0.594
Clock (m)	1.074	0.384	0.498
Instantaneous URE (m)	1.076	0.418	0.527

Table 1. Standard deviation of various SIS errors in meters grouped by Block Type

Spatial correlation of SIS errors

The three components of ephemeris error and the clock error are not necessarily independent from each other. We computed the correlation coefficients for every possible pair of R, A, C, and T, and the results show that significant correlation only exists among R, A, and T. Figure 5 shows these correlation coefficients for each satellite. The positive correlation between R and T is easy to understand, but the negative correlation between R and A was unexpected. The reason for the R-A correlation may be that the velocity of satellite is inversely proportional to the radius according to conservation of angular momentum, and a positive radial error may result in a negative velocity error and hence a negative alongtrack error.

Distribution of SIS errors

In addition to mean and standard deviation, SIS errors are further characterized in terms of distribution. Figure 6 shows the sample kurtosis of ephemeris errors, clock errors, instantaneous UREs, and worse-case UREs. It can be seen

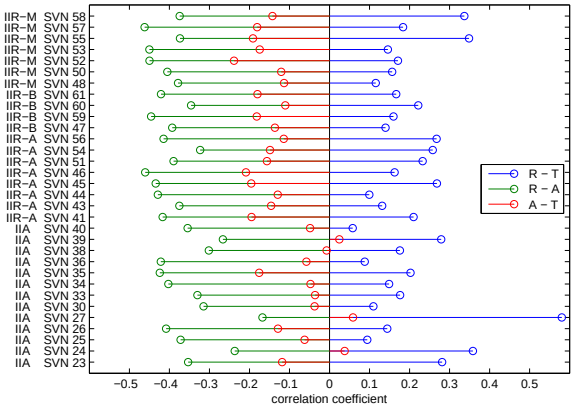

Figure 5. Correlation coefficients among radial errors, alongtrack errors, and clock errors.

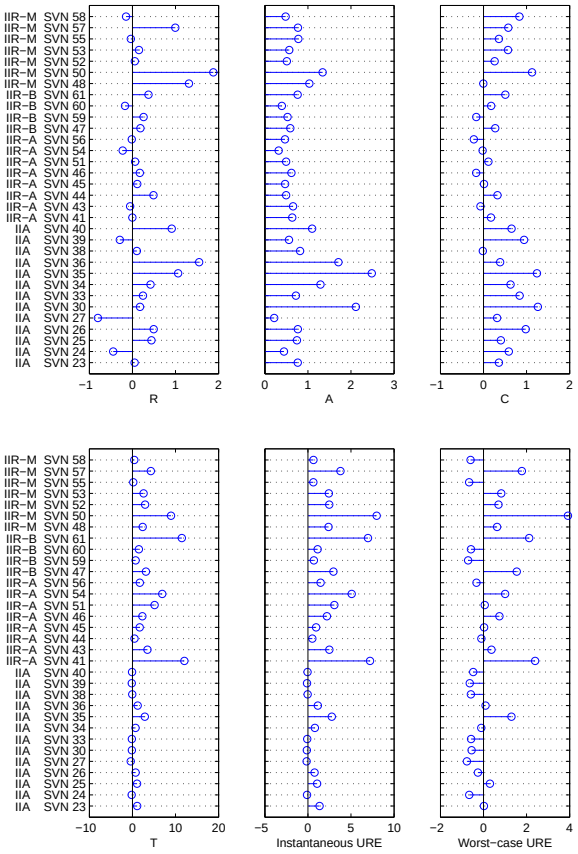

Figure 6. Kurtosis of various SIS errors

that as for ephemeris errors, all satellites have a super Gaussian distribution for alongtrack, and about a half satellites have a super Gaussian distribution for radial and crosstrack. Nevertheless, no ephemeris errors have a kurtosis greater than 3, which means that the tail is not very strong and a

normal distribution with inflated sigma should be able to overbound ephemeris errors. In contrast, clock errors, especially the clock errors of some young satellites, have very large kurtosis.

Another interesting phenomenon in Figure 6 is that worst-case URE generally has a lower kurtosis than instantaneous URE, which contradicts the common sense that "worst-case" should come with heavier tails. In fact, it is improbable for worst-case UREs to be close to zero. Therefore, unlike the unimodal continuous distributions such as normal distribution and Student's t-distribution which has one peak at the mean, the probability density function of worst-case UREs has two peaks. The two peaks boost the variance more than the 4th central moment, and hence reduce the kurtosis[4].

In addition to kurtosis, quantile-quantile (Q-Q) plot is graphical method to compare the empirical distribution of SIS errors with the standard normal distribution. Figure 7 shows three typical distributions: the sub-Gaussian distribution of IIA SVN 27 radial errors, the almost-Gaussian distribution of IIR-M SVN 55 clock errors, and the super-Gaussian distribution of IIR-M SVN 50 clock errors. It can be seen that even with negative kurtosis, the IIA SVN 27 radial errors still have relative heavy tails[5]. When the kurtosis is positive, the tails are much heavier. Therefore, a super-Gaussian distribution, such as Student's t-distribution, may fit the real data better.

Relation between rms URE and URA

As mentioned in Introduction, broadcast URA is intended to be a conservative representation of the expected rms behavior of the corresponding SIS UREs. Since URA is used extensively in not only position fix but also integrity monitoring, it is important to know how conservative URA is. Figure 8 plots the rms instantaneous URE and rms worst-case URE grouped by different broadcast URA. From the left subfigure, we can see that URA is truly conservative: for some old IIA satellites, URA is two times the expected rms URE; for most IIR and IIR-M satellites, URA is four times the expected rms URE. Furthermore, the rms worst-case URE in the right subfigure implies that even for the most unlucky user who always experiences largest URE, the user can still expect the rms URE much lower than URA. Besides, different satellites interpret URA very differently. For example, the rms instantaneous URE for IIA SVN 27 is around 1.3 meters despite the URA, whereas for IIR-M

[4]To understand this, consider an externa example, the Bernoulli distribution with $p = 1/2$, whose probability density function have two peaks, and the kurtosis is -2 [20].

[5]This apparent contradiction is because kurtosis depicts the normality of the majority 10^5 samples, and the strong upper and lower tails include no more than 50 samples.

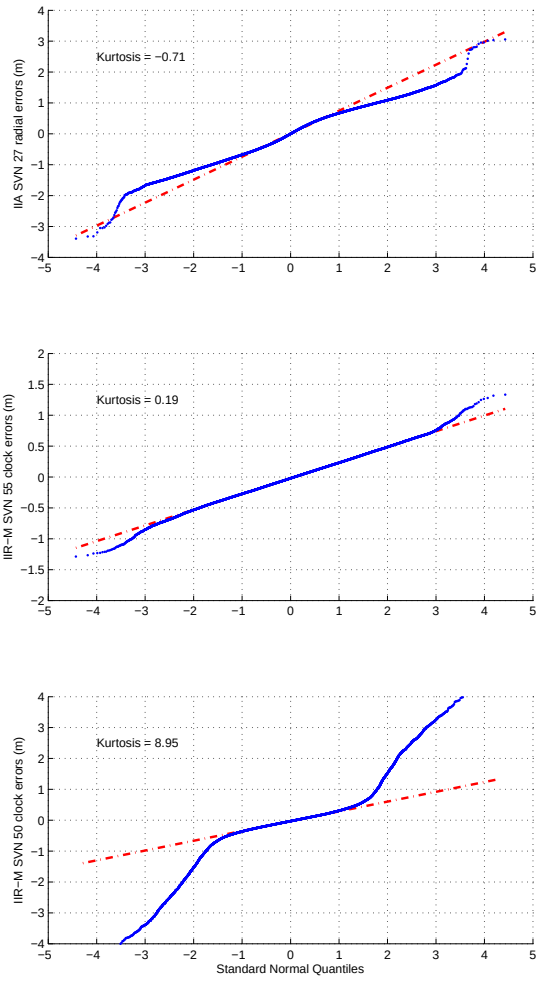

Figure 7. Q-Q plot of three typical SIS errors

SVN 50 different URA does indicate different levels of rms instantaneous URE.

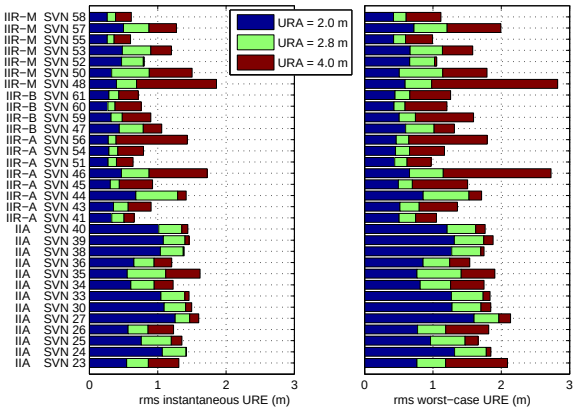

Figure 8. rms instantaneous URE and rms worst-case URE grouped by different broadcast URA.

Correlation among UREs of different satellites

In RAIM/ARAIM, a key assumption is that large UREs occur on several satellites simultaneously with very low probability. In other words, for an arbitrary user on the Earth, the correlation among the UREs of the satellites in view is expected to be close to zero. With this assumption, if UREs are close to normal, then the sum of their squares should be close to chi-square distributed. Therefore, multiple satellite monitoring in RAIM/ARAIM requires [10]

$$S = \sum_{i=1}^{k} \left(\frac{\mathrm{IURE}^i - \overline{\mathrm{IURE}}}{\mathrm{URA}^i} \right)^2 \leq K_{\mathrm{prob}}^2 = 50.2, \qquad (6)$$

where k is the number of the satellites in view. Here we consider only one case $k = 12$, which happened the most frequently in last three years. Because the removal of the common clock error in (6) causes loss of 1 degree of freedom (DoF), Figure 9 plots S against the chi-square distribution with 11 DoF.

The red dots in Figure 9 are computed with using the broadcast URA as the URA^i in (6). Clearly, the RAIM/ARAIM requirement was met as the maximum value is less than 15. Nevertheless, the red dots are far below the blue dash-dot line because, as mentioned in the previous subsection, the broadcast URAs are much greater than the standard deviation of UREs. Therefore, we replace the URA^i in (6) by the standard deviation of UREs, and get a result as the blue plus signs in Figure 9. It looks that the UREs of different satellites are highly correlated because the blue plus signs are high above the blue dash-dot line. However, the real UREs are not normally distributed, and on average they have a kurtosis of 1.5. Accordingly, we plot the green curve using the sum of several squared Student's t-random variables with $\nu = 8$ degrees of freedom. A Student's t-distribution with $\nu = 8$ has a kurtosis of 1.5, which can be seen as an approximation of the distribution of UREs. We tried the sum of 7, 8, 9, 10, 11, 12, or 13 squared such t-random variables, an

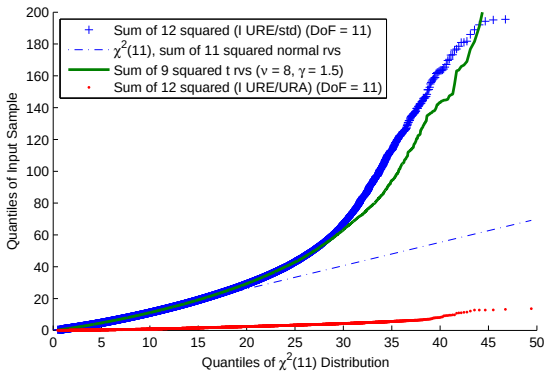

Figure 9. rms instantaneous URE and rms worst-case URE grouped by different broadcast URA.

the sum of 9 fits the majority of the blue plus signs best, as shown as the green curve. Therefore, a possible explanation is that correlation among UREs of different satellites cause a loss of 2 degrees of freedom.

SUMMARY

In this paper, we characterized core GPS SIS error behavior with respect to mean and standard deviation, spatial correlation, normality, relation between rms URE and URA, and correlation among different satellites. The ephemeris errors and clock errors are computed by comparing the broadcast ephemerides/clocks with the precise ones, followed by the generation of various SIS UREs. Outlier filter and robust statistics are employed to exclude anomalous satellite behaviors and statistical outliers. The data in recent three years are relatively stationary and hence analyzed. The results show that

- Mean of SIS errors are nonzero for several satellites, but still within ±0.2 times standard deviation;
- Younger satellites usually outperform older satellites;
- Clock performance dominates SIS URE performance;
- Radial errors, alongtrack errors, and clock errors are relatively strongly correlated;
- Clock errors and instantaneous UREs have heavier tails than normal distribution for about half of the satellites;
- URA is usually two times the expected rms URE for older satellites and four times for younger satellites;
- UREs of different satellites are slightly correlated, but still meets ARAIM's requirement.

ACKNOWLEDGMENTS

The authors gratefully acknowledge the support of the Federal Aviation Administration under Cooperative Agreement 08-G-007. This paper contains the personal comments and beliefs of the authors, and does not necessarily represent the opinion of any other person or organization.

REFERENCES

[1] P. Misra and P. Enge, *Global Positioning System: Signals, Measurements, and Performance*, 2nd ed. Lincoln, MA: Ganga-Jamuna Press, 2006.

[2] T. Creel, A. J. Dorsey, P. J. Mendicki, J. Little, R. G. Mach, and B. A. Renfro, "Summary of accuracy improvements from the GPS legacy accuracy improvement initiative (L-AII)," in *Proceedings of the 20th International Technical Meeting of the Satellite Division of The Institute of Navigation (ION GNSS 2007)*, Fort Worth, TX, September 2007, pp. 2481–2498.

[3] R. Schmid, M. Rothacher, D. Thaller, and P. Steigenberger, "Absolute phase center corrections of satellite and receiver antennas," *GPS Solutions*, vol. 9, pp. 283–293, 2005.

[4] G. Wong, R. E. Phelts, T. Walter, and P. Enge, "Characterization of signal deformations for GPS and WAAS satellites," in *Proceedings of the 23rd International Technical Meeting of The Satellite Division of the Institute of Navigation (ION GNSS 2010)*, Portland, OR, September 2010, pp. 3143–3151.

[5] US DoD, *Global Positioning System Standard Positioning Service Performance Standard*, 4th ed., September 2008.

[6] J. Blanch, M. J. Choi, T. Walter, P. Enge, and K. Suzuki, "Prototyping advanced RAIM for vertical guidance," in *Proceedings of the 23rd International Technical Meeting of The Satellite Division of the Institute of Navigation (ION GNSS 2010)*, Portland, OR, September 2010, pp. 285–291.

[7] J. Zumberge and W. Bertiger, "Ephemeris and clock navigation message accuracy," in *Global Positioning System: Theory and Applications*, B. Parkinson, J. Spilker, P. Axelrad, and P. Enge, Eds. Washington, DC: American Institute of Aeronautics and Astronautics, 1996, vol. I, pp. 585–699.

[8] R. B. Langley, H. Jannasch, B. Peeters, and S. Bisnath, "The GPS broadcast orbits: an accuracy analysis," in *33rd COSPAR Scientific Assembly*, Warsaw, Poland, July 2000.

[9] D. M. Warren and J. F. Raquet, "Broadcast vs. precise GPS ephemerides: a historical perspective," *GPS Solutions*, vol. 7, pp. 151–156, 2003.

[10] T. Walter, J. Blanch, and P. Enge, "Evaluation of signal in space error bounds to support aviation integrity," in *Proceedings of the 22nd International Technical Meeting of The Satellite Division of the Institute of Navigation (ION GNSS 2009)*, Savannah, GA, September 2009, pp. 1317–1329.

[11] J. C. Cohenour and F. van Graas, "GPS orbit and clock error distributions," *NAVIGATION, Journal of the Institute of Navigation*, acceptted April 2009.

[12] L. Heng, G. X. Gao, T. Walter, and P. Enge, "GPS ephemeris error screening and results for 2006–2009," in *Proceedings of the 2010 International Technical Meeting of the Institute of Navigation (ION ITM 2010)*, San Diego, CA, January 2010, pp. 1014–1022.

[13] ——, "GPS signal-in-space anomalies in the last decade: Data mining of 400,000,000 GPS navigation messages," in *Proceedings of the 23rd International Technical Meeting of The Satellite Division of the Institute of Navigation (ION GNSS 2010)*, Portland, OR, September 2010, pp. 3115–3122.

[14] J. M. Dow, R. E. Neilan, and C. Rizos, "The international GNSS service in a changing landscape of global navigation satellite systems," *Journal of Geodesy*, vol. 83, pp. 689–689, 2009.

[15] National Geospatial-Intelligence Agency GPS Division, Accessed November 2010. [Online]. Available: http://earth-info.nga.mil/GandG/sathtml/

[16] B. Wiley, D. Craig, D. Manning, J. Novak, R. Taylor, and L. Weingarth, "NGA's role in GPS," in *Proceedings of the 19rd International Technical Meeting of The Satellite Division of the Institute of Navigation (ION GNSS 2006)*, Fort Worth, TX, September 2006, pp. 2111–2119.

[17] S. S. Shapiro and M. B. Wilk, "An analysis of variance test for normality (complete samples)," *Biometrika*, vol. 52, no. 3-4, pp. 591–611, 1965.

[18] H. W. Lilliefors, "On the Kolmogorov-Smirnov test for normality with mean and variance unknown," *Journal of the American Statistical Association*, vol. 62, no. 318, pp. 399–402, 1967.

[19] C. M. Jarque and A. K. Bera, "Efficient tests for normality, homoscedasticity and serial independence of regression residuals," *Economics Letters*, vol. 6, no. 3, pp. 255 – 259, 1980.

[20] B. S. Chissom, "Interpretation of the kurtosis statistic," *The American Statistician*, vol. 24, no. 4, pp. 19–22, 1970.

[21] R. Schmid, P. Steigenberger, G. Gendt, M. Ge, and M. Rothacher, "Generation of a consistent absolute phase-center correction model for GPS receiver and satellite antennas," *Journal of Geodesy*, vol. 81, pp. 781–798, 2007.